Statistical distribution of factors and factor images in factor analysis of medical image sequences

I Buvat†, H Benali and R Di Paola

U494 INSERM, CHU Pitié-Salpêtrière, 91 Boulevard de l'Hôpital, 75 634 Paris Cedex 13, France

Abstract. From a time or energy image sequence, factor analysis of medical image sequences (FAMIS) estimates factors, representing kinetics or spectra in a given physiological compartment, and associated factor images, showing the compartments corresponding to each curve. In this paper, we show that the statistical properties of factor images and associated factors can be determined using a well known result from elementary probability theory. Numerical experiments are conducted to demonstrate that the variance observed in factor images can be predicted when the statistical properties of the original data are known. It is shown how these theoretical results can be used to relax the non-negativity constraints during FAMIS oblique analysis and to improve the quantitative interpretation of the factor images by associating a confidence interval with each pixel value.

1. Introduction

Factor analysis of medical image sequences (FAMIS) is a powerful method for estimating kinetics and associated compartments from a temporal image sequence (e.g. Barber 1980, Di Paola *et al* 1982, Houston and Sampson 1997, Samal *et al* 1987). It has also been demonstrated to be useful for scatter correction in planar scintigraphy and single photon emission computed tomography (SPECT) by means of the analysis of spectral image sequences (Buvat *et al* 1995). From an image sequence, FAMIS estimates a small number (typically two to four) of curves (kinetics or spectra), termed factors, and associated factor images (representing compartments), describing the image sequence using an underlying linear model. For instance, in the case of dynamic ^{13}N ammonia PET studies, right ventricular, left ventricular and myocardial compartments can be separated and the factors correspond to the time activity curves (TAC) associated with each compartment (Wu *et al* 1995). For SPECT scatter correction, a compartment represents the image of primary photons while the associated curve is the scatter-free spectrum. The other compartments represent scatter images and are associated with scatter spectra (Buvat *et al* 1995).

One issue which has not been studied so far concerns the statistical properties of the factors and factor images. As the factors and factor images can be the input of further processing, such as compartmental analysis for time series processing or tomographic reconstruction for SPECT scatter correction, determining the statistical properties of the signal in the factors and factor images would be useful, for instance, to associate a confidence interval with each pixel value in the factor images or with each curve point in the factors.

† E-mail address: buvat@imed.jussieu.fr

The importance of associating confidence intervals with the factor analysis parameters has already been underlined (Samal *et al* 1991).

In this paper, we derive the statistical properties of factors and factor images using a well known result from elementary probability theory. Analytical simulations demonstrate that the variance of each pixel value in the factor images can actually be predicted from the original image sequence. It is shown how these results can be used to introduce the notion of confidence interval when interpreting factor images and to take into account the uncertainty regarding pixel values and factor values for relaxing the non-negativity constraints used in the oblique rotation step involved in FAMIS.

2. Theory

In this section, the FAMIS model is presented and the method used to solve the model is described. The statistical properties of the factor images and factors are derived and it is shown how the oblique analysis can be modified to take into account these statistical properties.

2.1. The FAMIS model

Using a unified formalism (Benali *et al* 1994), the FAMIS model can be written

$$x_{ij} = \frac{x_{..}}{K} \sum_{k=1}^{K} \tilde{a}_k(i) \tilde{f}_k(j) + e_{ij}. \tag{1}$$

In this expression, x_{ij} is the signal intensity of pixel i in image j of the sequence and e_{ij} is a random error, corresponding to measurement noise. The total signal intensity in the image sequence $x_{..}$ is defined by

$$x_{..} = \sum_{i=1}^{N} \sum_{j=1}^{P} x_{ij}$$

where N is the number of pixels in an image and P is the number of images in the sequence. Equation (1) states that the curve $x_i = \{x_{ij}\}_{j=1,P}$, termed trixel i, associated with each pixel i can be expressed as a linear combination of a small number K of fundamental curves $\{\tilde{f}_k(j)\}_{j=1,P}$ weighted by the coefficients $\tilde{a}_k(i)$. A symmetrical (or dual) interpretation of this model (Benali *et al* 1994, Samal *et al* 1988) is that each image $x_j = \{x_{ij}\}_{i=1,N}$ of the sequence can be expressed as a linear combination of K fundamental images $\{\tilde{a}_k(i)\}_{i=1,N}$, representing compartments, weighted by coefficients $\tilde{f}_k(j)$.

The problem to be solved is: given the initial image sequence $\{x_{ij}\}_{i=1,N \text{ and } j=1,P}$ and assuming that K is known, find the fundamental images $\{\tilde{a}_k(i)\}_{i=1,N}$ and the associated fundamental curves $\{\tilde{f}_k(j)\}_{j=1,P}$. The estimated fundamental images are termed factor images, while the estimated fundamental curves are termed factors.

2.2. Solution of the model

Solving the model involves several steps which have been described and discussed in detail previously (see, for instance, Di Paola *et al* 1982, Frouin *et al* 1992). Only the relationships necessary for the demonstrations of this paper will be presented here. The other steps involved in FAMIS will only be briefly mentioned.

2.2.1. Pre-processing. The first step of FAMIS consists of grouping pixels together, usually using a geometrical pattern (e.g. 4×4 blocks of pixels), in each image of the sequence. This corresponds to using a coarser spatial sampling. All variables corresponding to this coarse spatial sampling will be denoted by an asterisk (*). To reduce the influence of noise and irrelevant background signal, a thresholding procedure is then performed, so that only trixels with an intensity $x_{i.}^*$ greater than a given threshold are further analysed. The trixel intensity $x_{i.}^*$ of trixel i is defined by

$$x_{i.}^* = \sum_{j=1}^{P} x_{ij}^*.$$

2.2.2. Orthogonal analysis. The second step of FAMIS solves a statistical model, the fixed effect model (Caussinus 1986), to estimate the noise-free component $x_{ij}^* - e_{ij}^* = \tilde{x}_{ij}^*$ (Benali *et al* 1993). The fixed effect model states that the observed signal x_{ij}^* is the sum of a fixed component (non-random or noise-free component) $\tilde{x}_{ij}^*$ and a random error e_{ij}^*. Solving the fixed effect model yields a low-dimensional subspace of $\mathbb{R}^P$, called study subspace $\mathbb{S}$, such that the projection of the original trixel x_{ij}^* onto this subspace gives the noise-free component $\tilde{x}_{ij}^*$. The study subspace $\mathbb{S}$ is obtained using an orthogonal decomposition performed with the appropriate metrics, derived from the statistical properties of the original data. For instance, it has been shown that for scintigraphic data which are Poisson distributed, the appropriate orthogonal decomposition was that of correspondence analysis (Benali *et al* 1993). In that case, the noise-free trixels are given by

$$\tilde{x}_{ij}^* = \frac{x_{i.}^* x_{.j}}{x_{..}} + \sum_{q=1}^{K-1} \frac{x_{i.}^* x_{.j}}{x_{..}} \frac{1}{\sqrt{\lambda_q}} \varphi_q(j) \psi_q^*(i) \tag{2}$$

where the eigenvalues λ_q, the eigenvectors φ_q and the eigenimages ψ_q^* result from the orthogonal decomposition and

$$x_{.j} = \sum_{i=1}^{N} x_{ij}.$$

The result of the orthogonal decomposition gives a basis of $K - 1$ orthogonal eigenvectors $\{\varphi_q(j)\}_{j=1,P}$ which span the study subspace $\mathbb{S}$ in which the noise-free trixels can be estimated.

2.2.3. Oblique analysis. The next step, called oblique analysis, estimates the fundamental curves $\{\tilde{f}_k(j)\}_{j=1,P}$ and the fundamental images $\{\tilde{a}_k^*(i)\}_{i=1,N}$. The basic hypothesis is that the fundamental curves and the fundamental images belong to the study space $\mathbb{S}$ resulting from the orthogonal analysis. Two dual models can be considered (Benali *et al* 1994): a model pertaining to the fundamental curves (called the curve model) and a model pertaining to the fundamental images (called the image model) (see the appendix). Either model can be solved in an iterative manner, using non-negativity constraints, normalization constraints and *a priori* knowledge (see the appendix). Briefly, the iterative procedure consists of starting with a first set of factors and in deriving the corresponding factor images given the trixel x_{ij}^*. These images are then modified to meet non-negativity, normalization and *a priori* constraints and, using these new images, the corresponding factors are deduced. These new factors are modified to meet the non-negativity, normalization and *a priori* constraints and, after these modifications, new corresponding factor images are deduced.

This process is repeated and when it stops, either the factors or the factor images meeting the non-negativity, normalization and *a priori* constraints are known.

2.3. Statistical properties of factor images and factors

2.3.1. Factor images. At the end of the iterative process, assuming the factors are known, the corresponding factor images are deduced by projecting the original noisy trixels x_{ij} onto the factors $\{\tilde{f}_k(j)\}_{j=1,P}$. The projection operation reads

$$a_k(i) = \sum_{j=1}^{P} x_{ij} \tilde{f}'_k(j) \tag{3}$$

where the $\tilde{f}'_k(j)$ are the elements of the matrix $\tilde{F} \ (\tilde{F}^t \tilde{F})^{-1}$ and $\tilde{F}$ is the $P \times K$ matrix of the $\{\tilde{f}_k(j)\}$. The statistical properties of the factor images $a_k(i)$ can be derived from equation (3). Indeed, $a_k(i)$ can be written

$$a_k(i) = \sum_{j=1}^{P} (\tilde{x}_{ij} + e_{ij}) \tilde{f}'_k(j) = \sum_{j=1}^{P} \tilde{x}_{ij} \tilde{f}'_k(j) + \sum_{j=1}^{P} e_{ij} \tilde{f}'_k(j) = \tilde{a}_k(i) + \varepsilon_{ki}. \tag{4}$$

In this expression, the first term $\tilde{a}_k(i)$ is the non-random part, while the second term is random, because of the random nature of the original signal x_{ij}. In the case of Poisson data x_{ij} of parameter v_{ij}, as when dealing with scintigraphic data, two cases can be considered:

(i) If x_{ij} is greater than 30, x_{ij} can be considered as Gaussian distributed. $a_k(i)$ is therefore a linear combination of Gaussian variables and is Gaussian distributed.

(ii) If x_{ij} is less than 30, x_{ij} is Poisson distributed. However, if P is large enough ($P \geqslant 30$), the central limit theorem applies so that the sum over j of random errors with the same law is Gaussian distributed. The resulting $a_k(i)$ is therefore Gaussian distributed.

The third case, corresponding to $x_{ij} < 30$ and $P < 30$, will be studied in section 4 and further commented upon in the discussion.

If $a_k(i)$ is Gaussian distributed, it is entirely characterized by its first- and second-order moments. Using equation (3), the variance of $a_k(i)$ can be expressed as a function of the variance of the original data by

$$\text{Var}[a_k(i)] = \sigma^2(i) = \sum_{j=1}^{P} \text{Var}[x_{ij}] \tilde{f}'^2_k(j). \tag{5}$$

There are no covariance terms since the x_{ij} are assumed to be independent variables. Equation (5) corresponds to the well known result from elementary probability theory stating that the variance of a weighted sum of random variables is the squared weighted sum of the variances of the variables. In our context, this means that for a set of factors $\tilde{f}_k(j)$, the variance of the factor images can be deduced from the variance of the original data. For a Poisson variable x_{ij} of parameter v_{ij}, $\text{Var}[x_{ij}] = v_{ij}$. A classical estimate for v_{ij} is x_{ij} and therefore equation (5) reduces to

$$\text{Var}[a_k(i)] = \sum_{j=1}^{P} x_{ij} \tilde{f}'^2_k(j). \tag{6}$$

Using this relationship, a variance value can be associated with the pixel contents of each factor image.

2.3.2. Factors. Considering the dual formalism of FAMIS, and assuming that the factor images $\tilde{a}_k(i)$ are known at the end of the iterative process, the factors can be deduced by

$$f_k(j) = \sum_{i=1}^{N} x_{ij} \tilde{a}'_k(i) \tag{7}$$

where the $\tilde{a}'_k(i)$ are the elements of the matrix $\tilde{A}\,(\tilde{A}^t \tilde{A})^{-1}$ and $\tilde{A}$ is the $N \times K$ matrix of the $\tilde{a}_k(i)$. The statistical properties of the factors can then be determined using a similar demonstration to that used to derive the statistical properties of the factor images (equation (4)). If $x_{ij} \geqslant 30$ or N large enough, the latter always being true, we obtain that (i) the values $f_k(j)$ are Gaussian distributed and (ii) the variance $\mathrm{Var}[f_k(j)]$ of $f_k(j)$ is

$$\mathrm{Var}[f_k(j)] = \sigma^2(j) = \sum_{i=1}^{N} \mathrm{Var}[x_{ij}]\tilde{a}'^2_k(i) \tag{8}$$

which reduces to

$$\mathrm{Var}[f_k(j)] = \sum_{i=1}^{N} x_{ij}\tilde{a}'^2_k(i) \tag{9}$$

for Poisson data.

Note that depending on what one is interested in (variance of the factor images or variance of the factors), one should assume either that the factors are not random to deduce the statistical properties of the associated factor images given the random original trixels x_{ij}, or that the factor images are not random to determine the variance of the associated factors given the random original data.

2.4. Practical implications

Knowing the statistical properties of the factors and factor images can be taken advantage of in at least two different ways: (i) to introduce the notion of confidence intervals when interpreting the factor images and (ii) to introduce the notion of confidence intervals in the iterative procedure of oblique analysis.

2.4.1. Associating a confidence interval to the factor image pixel values. Equation (9) shows that, for given factors $\tilde{f}_k(j)$, the variance of each pixel value in the factor images can be deduced. As the factor image pixel values are Gaussian distributed with a known variance $\mathrm{Var}[a_k(i)] = \sigma^2(i)$, a confidence interval $[a_k(i) - c\sigma(i); a_k(i) + c\sigma(i)]$ can be associated with each pixel value $a_k(i)$, where c depends on the type I error. For instance, for a type I error $\alpha = 0.05$, $c = 1.96$. A straightforward use of this confidence interval can be a thresholding procedure, in which all pixel values which are not significantly different from zero are set to zero. In other words, if $[a_k(i) - c\sigma(i)] \leqslant 0$ then $a_k(i) = 0$. The practical consequences of such an operation will be illustrated in section 4.

2.4.2. Relaxing the non-negativity constraints in the oblique analysis. In the oblique analysis, at each iteration, factor images are calculated using equation (3), except that the preprocessed trixels x^*_{ij} are used instead of the original trixels x_{ij}. Therefore, the variance $\mathrm{Var}[a^*_k(i)] = \sigma^2(i)$ of the factor images $\{a^*_k(i)\}_{i=1,N}$ is given by

$$\mathrm{Var}[a^*_k(i)] = \sum_{j=1}^{P} \mathrm{Var}[x^*_{ij}]\tilde{f}'^2_k(j).$$

As a result, a confidence interval $[a_k^*(i) - c\sigma(i); a_k^*(i) + c\sigma(i)]$ can be associated with each pixel value $a_k^*(i)$. Given this confidence interval, the non-negativity constraints, which conventionally consist of setting to zero all pixel values less than zero, can be relaxed so that only the pixel values *significantly* less than zero are set to zero, i.e.

$$\text{if } [a_k^*(i) + c\sigma(i)] < 0 \qquad \text{then} \qquad a_k^*(i) = 0.$$

Similarly, using equation (8), a confidence interval $[f_k(j) - c\sigma(j); f_k(j) + c\sigma(j)]$ can be associated with each factor value $f_k(j)$. Given this confidence interval, the non-negativity constraints, which conventionally consist of replacing by zero all factor values less than zero, can be relaxed so that only the factor values *significantly* less than zero are set to zero, i.e.

$$\text{if } [f_k(j) + c\sigma(j)] < 0 \qquad \text{then} \qquad f_k(j) = 0.$$

3. Materials and methods

Numerical simulations have been performed (i) to check the validity of the theoretical results regarding the statistical properties of the factor images and to study the domain of validity of these results and (ii) to investigate the practical consequences of the theoretical results.

3.1. Statistical properties of the factor images

3.1.1. Statistical distribution. A two-compartment phantom (figure 1(*a*)) was used to study the nature of noise in the factor images. The phantom consisted of two non-overlapping homogeneous rectangles A1 and A2, with an area of 1200 pixels each. The two fundamental curves $\tilde{f}_1$ and $\tilde{f}_2$ associated with these fundamental images were a constant curve and a monotonically increasing curve. The same contribution was given to each compartment, i.e. the total signal intensity in each compartment was the same. Using these fundamental components, five image sequences were created by varying the total number of counts $x_{..}$ and the number of images P in the sequence. The parameters of the simulations are summarized in table 1. Poisson noise was added to each image. For each $x_{..}$, the mean value of x_{ij} in the sequence is given in table 1. Each image sequence was processed with FAMIS using the following protocol: 4×4 pixel grouping; all trixels with intensity greater than 30 were analysed; the two factors were set by projecting the known fundamental curves into the study space, so that no variability due to an arbitrary number of iterations would be introduced. Setting the factors guaranteed that they would be very close to the true fundamental curves. No iterations were performed. For each analysis, two factor images were obtained, one corresponding to each compartment.

a   b
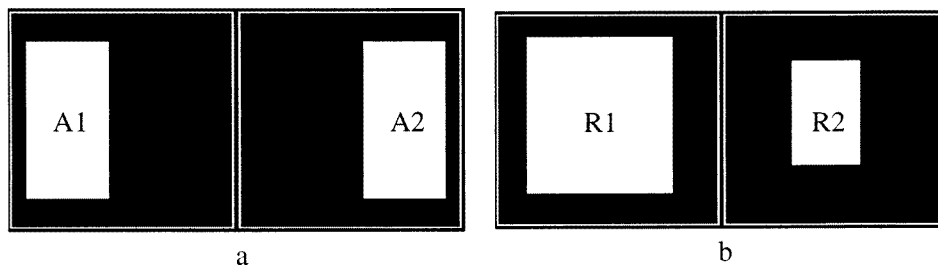
Figure 1. Fundamental images used for (a) simulations 1 to 6, (b) simulation 7.

Table 1. Characteristics of the different simulations.

Simulation no	a_1	a_2	$\tilde{f}_1$	$\tilde{f}_2$	$x_{..}$	Mean x_{ij}	P
1	A1	A2	$\tilde{f}_1(j) = C1$	$\tilde{f}_2(j) = 2j$	5 600 000	77	30
2	A1	A2	$\tilde{f}_1(j) = C1$	$\tilde{f}_2(j) = 2j$	720 000	10	30
3	A1	A2	$\tilde{f}_1(j) = C1$	$\tilde{f}_2(j) = 4j - 2$	2 800 000	77	15
4	A1	A2	$\tilde{f}_1(j) = C1$	$\tilde{f}_2(j) = 4j - 2$	360 000	10	15
5	A1	A2	$\tilde{f}_1(j) = C1$	$\tilde{f}_2(j) = 12j - 6$	120 000	10	5
6	A1	A2	$\tilde{f}_1(j) = 300\exp(-0.1j)$	$\tilde{f}_2(j) = 100j^{0.25}$	2 800 000	39	30
7	R1	R2	$\tilde{f}_1(j) = 300\exp(-0.1j)$	$\tilde{f}_2(j) = 100j^{0.25}$	2 800 000	42	30

As the simulated compartments presented a uniform signal and because the estimated factors were very close to the true fundamental curves, the number of counts in the factor images should theoretically be identical in each pixel of a compartment. The statistical distribution of noise in the factor images could therefore be investigated by looking at the distribution of pixel values in each compartment. The Gaussian nature of noise in each compartment was tested using a Kolmogorov–Smirnov test (Kendall and Stuart 1979).

3.1.2. Variance in the factor images. To test whether the variance observed in the factor images could be predicted by the theoretical relationship (6), a 'variance image' was calculated using equation (6) for each factor image. Using these variance images, the mean variance value in each compartment was calculated. This mean value gave the *theoretical* estimate of the variance of the Gaussian distribution associated with the compartment. On the other hand, using the factor images, the mean and variance of the pixel values were calculated for each compartment. This gave the *observed* variance in the factor images. The theoretical and observed variance values were then compared. This comparison was performed for the five numerical simulations described above. In addition, as the theory predicts that the variance depends on the factor shape, another simulation with different curve shapes was performed. An image sequence was created by using the fundamental distributions A1 and A2 (figure 1(*a*)) associated with curves $\tilde{f}_1(j) = 300\exp(-0.1j)$ and $\tilde{f}_2(j) = 100j^{0.25}$ respectively (simulation 6 in table 1). This sequence was processed using the same FAMIS protocol as that described above. Equation (6) also indicates that the variance in the factor images is a function of the estimated factors and is not a function of the true underlying fundamental curves. To check whether this was indeed the case, another simulation (simulation 7 in table 1) was performed so that the estimated factors would be biased. The fundamental spatial distributions were two overlapping rectangles R1 and R2 (figure 1(*b*)) and the associated curves were the same as those used for simulation 6. Using this image sequence, two FAMIS were performed. The same clustering and thresholding procedures as those described above were used. In the first analysis, the two factors were set using the known fundamental curves and no iterations were performed. In the second analysis, the factors were not set *a priori* and five iterations were used to estimate the fundamental curves.

3.2. Practical implications

3.2.1. Associating a confidence interval with the factor image pixel values. For all FAMIS which were performed, each factor image was thresholded so that all pixels with values not significantly different from zero were set to zero. The number of non-zero pixels that should theoretically be zero was noted, before and after thresholding the factor images.

3.2.2. Relaxing the non-negativity constraints in the oblique analysis. A simulation was performed using three rectangular non-overlapping compartments, of 240 pixels each, with a uniform signal intensity. The curves associated with these compartments were $\tilde{f}_1(j) = 2j$, $\tilde{f}_2(j) = 300 \exp(-0.1j)$ and $\tilde{f}_3(j) = 100 j^{0.25}$, for $j = 1$ to 30 and the three compartments represented 33%, 34% and 33% of the total signal intensity respectively. Using these compartments and curves, a sequence of 30 images with 400 000 counts in total was created and Poisson noise was added. The mean number of counts per pixel was 18. Two FAMIS were performed, each using a 4×4 pixel grouping and analysing trixels with intensity greater than 30. In the first analysis, factors were estimated in an iterative manner using the conventional non-negativity constraints (without taking into account the confidence interval associated with factor and factor image values) and 37 iterations were performed. The second analysis was also performed using 37 iterations, but non-negativity constraints were relaxed so that only the values significantly less than zero were set to zero during the oblique analysis. In both analyses, the resulting factor images were thresholded using the variance values, so that all values not significantly different from zero were set to zero.

4. Results

4.1. Statistical properties of the factor images

4.1.1. Statistical distribution. The mean and standard deviation of the signal in each compartment of the factor images are summarized in table 2 for the different simulations. The critical value for the Kolmogorov–Smirnov test was 0.039 at $p = 0.05$. In all cases, the observed statistics was less than 0.039, meaning that the statistical distribution of the signal in each compartment did not significantly depart from a Gaussian distribution. As an example, the histogram of pixels values in compartment 1 for simulation 1 is shown in figure 2.
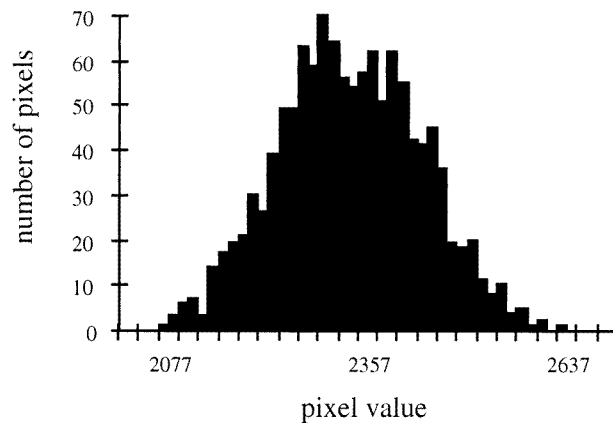
Figure 2. Histogram of pixel values in compartment 1 for simulation 1.

4.1.2. Variance in the factor images. The variances measured in the factor images for the different compartments and simulations are given in table 3, as a function of the variance values predicted from the theory (equation (6)). For the second FAMIS performed on simulation 7, where the factors were not set *a priori*, the factors and factor images

Table 2. Mean signal and associated standard deviation in each compartment (cpt) and associated Kolmogorov–Smirnov (KS) test values.

| Simulation no	cpt 1 (mean ± sd)	KS test	cpt 2 (mean ± sd)	KS test
1	2324 ± 99	0.004 03	2324 ± 85	0.003 03
2	300 ± 36	0.002 00	298 ± 31	0.003 03
3	1163 ± 67	0.003 10	1162 ± 62	0.004 40
4	150 ± 25	0.006 13	148 ± 21	0.006 43
5	50 ± 14	0.009 13	50 ± 13	0.005 80

Table 3. Observed variance and variance predicted from the theory in the different compartments (cpt) for the different simulations.

| Simulation no	cpt	Observed variance	Variance predicted from theory
1	1	9893	9743 ± 298
1	2	7183	7491 ± 204
2	1	1290	1265 ± 108
2	2	975	966 ± 75
3	1	4432	4661 ± 197
3	2	3793	3506 ± 145
4	1	638	602 ± 75
4	2	445	449 ± 49
5	1	205	207 ± 44
5	2	168	155 ± 30
6	1	2287	2378 ± 107
6	2	1762	1732 ± 61
7—FAMIS 1	1	1608	1636 ± 523
7—FAMIS 1	2	3589	3782 ± 97
7—FAMIS 2	1—ROI 1	3485	3593 ± 128
7—FAMIS 2	1—ROI 2	1628	1671 ± 106
7—FAMIS 2	2	5831	6145 ± 157

were biased compared with the true fundamental structures (figure 3). In the first factor image, the theoretical and observed variance were compared in two different regions of interest (figure 4), while in the second factor image, they were compared only in a region corresponding to the second compartment. A plot of the observed variance against the theoretical variance for all simulations is shown in figure 5.

4.2. Practical implications

4.2.1. Associating a confidence interval to the factor image pixel values. The numbers of pixels with non-zero values in regions where there should theoretically be zero for the different factor images and simulations are given in table 4 before and after thresholding the factor images. Before thresholding, for the factor image representing mainly compartment k, there were a large number of non-zero pixels in the region corresponding to the other compartment. After thresholding, this number was strongly reduced and there only remained between 0% and 4% of the non-zero pixels observed before thresholding.
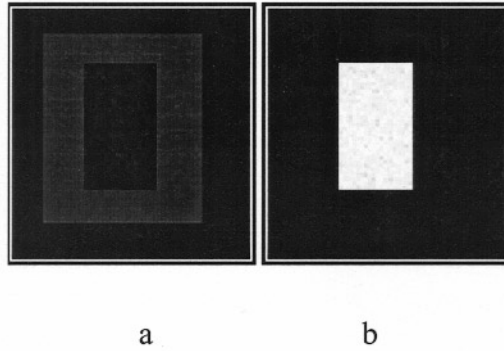
Figure 3. Factor images obtained for simulation 7 when not fixing the factors. The true compartments are shown in figure 1(*b*).
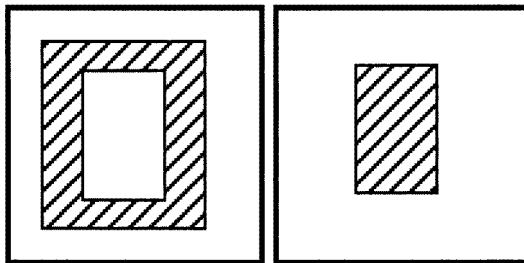
Figure 4. Regions of interest (hatched areas) used to calculate the variance in the biased factor images shown in figure 3(*a*).
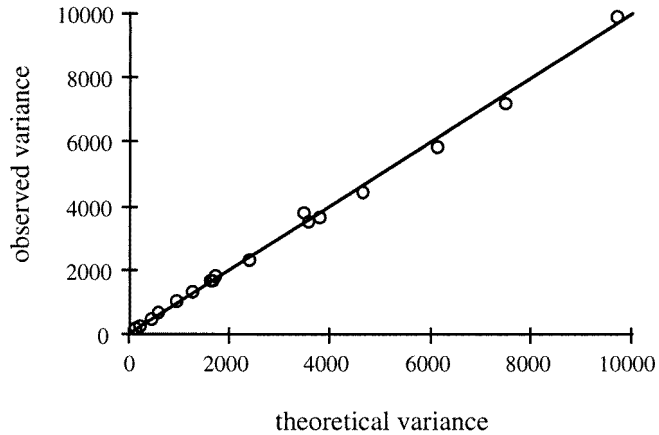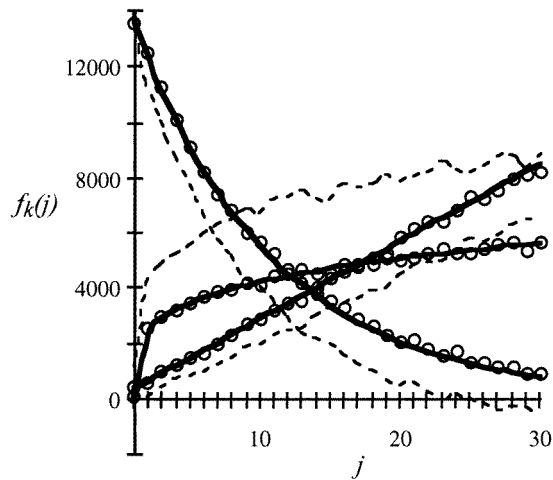

Figure 5. Observed variance in the factor images as a function of the variance predicted from the theory.

4.2.2. Relaxing the non-negativity constraints. The factors estimated using the two FAMIS performed for the three-compartment simulations are superimposed with the true fundamental curves in figure 6. When *not* relaxing the non-negativity constraints, the iterative algorithm actually diverged around iteration 30, yielding poor curve estimates

Table 4. Number of non-zero pixels in regions where there should be zero for the different simulations, before and after thresholding the factor images using the estimated variance values.

Simulation no	Image	No of non-zero values before thresholding	No of non-zero values after thresholding
1	1	1196	20
1	2	1190	24
2	1	1184	32
2	2	1183	44
3	1	1192	32
3	2	1183	26
4	1	1178	37
4	2	1182	35
5	1	1159	3
5	2	1153	30
6	1	1182	24
6	2	1191	31
7—FAMIS 1	1	0	0
7—FAMIS 1	2	1490	56

Figure 6. Estimated factors for the three-compartment simulations. Full curves: original fundamental curves. Broken curves: factors obtained when not using the relaxed non-negativity constraints. Open circles: factors estimated using the relaxed non-negativity constraints.

(broken curves). When relaxing the non-negativity constraints, the solution remained stable from iteration 30. For each factor image and each compartment, figure 7 shows the theoretical and the observed mean values for the two analyses, before and after thresholding the factor images, by taking into account the variance value associated with each pixel of the factor images. When not relaxing the non-negativity constraints, the mean number of counts was underestimated by 14% in compartment 1 (factor image 1), by 33% in compartment 2 (factor image 2) and by 5% in compartment 3 (factor image 3). In addition, before thresholding the factor images using the confidence intervals, there was substantial apparent signal in compartments 1 and 2 in factor image 3. Thresholding the factor images reduced this signal. When relaxing the non-negativity constraints during the oblique analysis, the
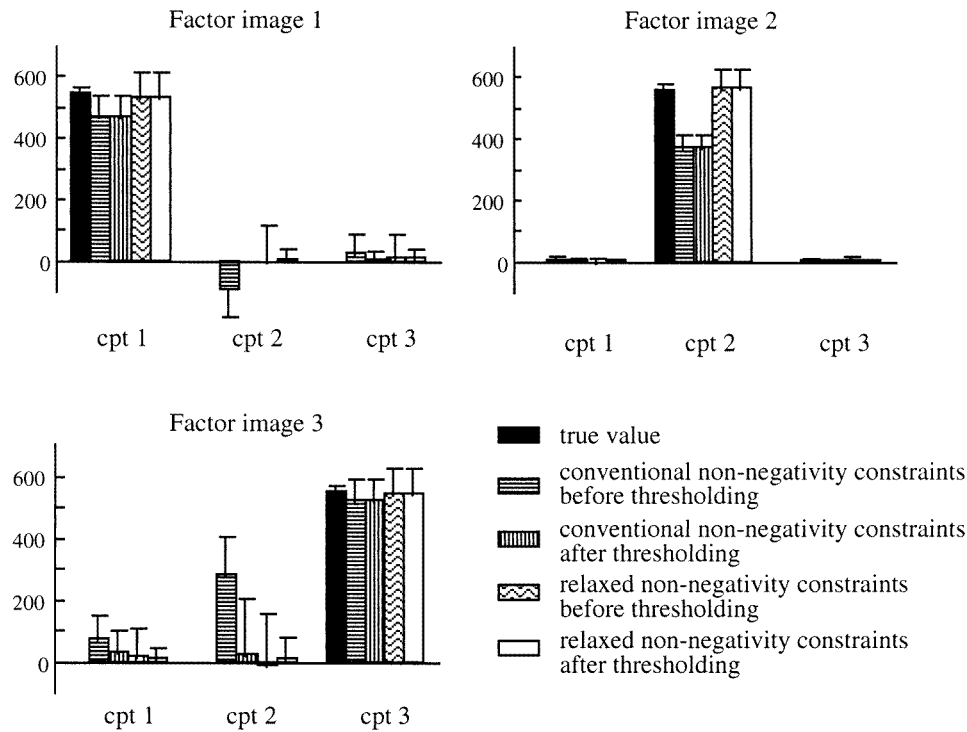
Figure 7. Mean values measured in the different compartments and the different factor images for the three-compartment simulation.

mean numbers of counts were underestimated by 2% in compartments 1 and 3, and it was overestimated by 2% in compartment 2. For the factor image k corresponding to compartment k, there was almost no signal in the other compartments.

5. Discussion

The aim of FAMIS is to estimate (time or energy) curves and associated compartments from an image sequence. Most often, the resulting factors and factor images are further analysed, either only visually, or for quantitative purpose. From a quantitative point of view, factors can be used for compartmental analyses (Samal *et al* 1993) or factor images can be used to estimate signal intensity in a given compartment. For interpreting factors or factor images quantitatively, it would therefore be useful to associate 'confidence intervals' with the factor values and with the factor image pixel values.

This paper derived the statistical properties of factors and factor images. The case of scintigraphic data for which the signal is Poisson distributed was considered in the simulations. However, equations (3) and (7) from which the statistical properties of factor images and factors are deduced apply whatever the statistical properties of the original data. For Gaussian data, for instance, equation (3) shows that the factor images would also be Gaussian. Characterizing the variance of the factors and factor images requires the variance of the original trixels x_{ij} to be known. In the case of Poisson data x_{ij} of parameters v_{ij}, the solution is trivial since $\text{Var}[x_{ij}] = v_{ij}$ which can be well approximated by x_{ij}. It is

therefore straightforward to calculate the variance values associated with pixel or factor value (equations (6) and (9)). For Gaussian data, the variance values could also be theoretically calculated using equations (5) and (8) provided one can estimate the variance of the original trixels x_{ij}. Note that equations (5) and (8) only apply when the noise e_{ij} associated with the original trixels x_{ij} is not spatially correlated, making the covariance terms equal to zero. In that case, equations (5) and (8) are nothing other than the elementary result from probability theory which states that the variance of a weighted sum of random variables is equal to the squared weighted sum of the variances of the variables. For spatially correlated noise, equations (5) and (8) would contain covariance terms which should be estimated to make calculation of the factor and factor image variance reliable. In the case of Poisson data, the numerical simulations demonstrated the validity of the theoretical results, namely that the signal is Gaussian distributed in the factor images (table 2 and figure 2), and that the variance associated with each pixel value can be predicted using equation (6) (table 3 and figure 5). The Gaussian nature of the signal in factor images is theoretically guaranteed if either x_{ij} or the number of images P is greater than 30. The experimental results showed that in agreement with the theory, the signal is Gaussian for $x_{ij} > 30$ even is P is low (simulation 3), or for $P \geqslant 30$ if $x_{ij} < 30$ (simulation 2). As a result, the signal is also Gaussian when both $x_{ij} \geqslant 30$ and $P \geqslant 30$ (simulation 1). Furthermore, it was found that the signal in the factor images remained Gaussian when both P and x_{ij} were low (simulations 4 and 5). This is probably because both x_{ij} and P values contribute to the convergence towards the Gaussian asymptotic results. From a practical point of view, factor images are therefore always Gaussian for scintigraphic data. Another important characteristic is that the variance associated with each pixel value in the factor images does not depend on the true fundamental curves. It is entirely determined by the variance of the original trixels x_{ij} and by the estimated factors $\tilde{f}_k$. If the factors are biased estimates of the underlying fundamental curves (simulation 7, FAMIS 2), the variance values depend on the bias (since they are calculated from the estimated factors), but can be estimated without estimating the bias (table 3). This means that variance values can be systematically associated with factor images, even when the bias that may affect the factors is unknown (which is what happens most often).

The same theoretical derivations apply for associating variance values with factors (equations (7) and (8)). For Poisson data, factors are therefore Gaussian distributed, since the number of trixels N is always greater than 30. For Gaussian initial data, factors would also be Gaussian distributed. A confidence interval can be associated with each factor value using equation (8). Again, variance can be associated with factors without knowing the bias that may affect the factor images.

Note that if the statistical distribution of the original data was unknown, or if the statistical distribution of the factor images or factors was unknown, the only way to estimate the variance of the factor analysis parameters would be to replicate the same experiment a large number of times.

It is important to underline that one cannot associate variance values with factors *and* factor images simultaneously. Indeed, either the factors are assumed to be non-random and the variance of the factor images is deduced from the projection of the random original trixels onto the non-random factors, or the factor images are assumed to be non-random and the variance of the factors is deduced from the projection of the random original trixels onto the images.

We have presented two applications for which knowledge of the statistical properties of factors and factor images can be used to advantage. A straightforward use of the variance associated with each pixel value in the factor images is to determine whether the pixel value

is significantly different from zero. If it is not, it can be replaced by zero. This thresholding operation greatly reduced the signal present in the factor images in regions where signal should be zero (table 4). On the other hand, it did not affect signal in regions where it was high enough (figure 7) and therefore significant. The relevance of thresholding may be questionable in regions of intrinsic low-intensity signal, where weak signal could be partially cancelled by thresholding. To make thresholding more robust, it might be worth using a spatial model during the thresholding operation. For instance, deciding whether a pixel should be set to zero could depend not only on the pixel value and associated variance, but also on the values and variances observed in neighbouring pixels.

A second application concerns the oblique analysis procedure. The conventional oblique analysis algorithm is based on non-negativity constraints: negative values in factors and in factor images are set to zero in turn in the iterative algorithm until the solution meets the non-negativity constraints 'reasonably well'. This algorithm can be seen as an iterative forward/backward estimation technique. Calculation of the factor images corresponds to a forward estimation, given the original trixels and assuming that the factors are known. The backward step estimates the factors given the original random trixels and the known factor images. At each step, non-negativity constraints should ensure that the number of negative values in factors or factor images decrease. A flaw in this approach, however, is that all negative values are set to zero, whether they are significantly negative or not. As shown using the three-compartment simulation, this can cause the algorithm to diverge. On the other hand, using the 'relaxed' non-negativity constraints to account for the confidence interval associated with each factor or factor image value prevents the algorithm from diverging. A solution is achieved where all negative values are not significantly different from zero so that neither factor images nor factors are modified. Another related, although less dramatic, phenomenon was observed in the case of trixels with a high level of noise (typically x_{ij} less than 30). In such cases, the cloud of points in the study space (i.e. the β_{kq} coordinates, see the appendix) corresponding to a compartment is spread out because of noise. For each compartment, the conventional oblique analysis algorithm with *strict* non-negativity constraints finds a solution corresponding to the extreme points of the clouds, i.e. at the edge of the clusters corresponding to the different compartments, while the true solution rather lies at the centre of gravity of each cloud of points. Using the relaxed non-negativity constraints prevents this effect and gives a solution inside the cloud of points, i.e. close to the true solution.

6. Conclusion

We have demonstrated that the statistical properties of factors and factor images can be theoretically derived from the statistical properties of the initial data. Using simulations, we showed that in the case of Poisson data, the experimental results were consistent with those predicted by the theory. The advantages of accounting for the variance associated with factor values or factor image pixel values were demonstrated in two instances: for thresholding factor images so that false signal coming from noise can be removed, and for relaxing the non-negativity constraints in the oblique analysis procedure involved in FAMIS. This relaxation method has been shown to prevent the iterative oblique analysis algorithm from diverging on a numerical simulation. Other potential applications of the results presented in this paper include adaptive factor image restoration based on the statistical properties of the factor images. Further theoretical studies will also concern the variance estimates of factors and factor images for original data with spatially correlated noise.

Appendix

In this appendix, we present the FAMIS oblique analysis model and the algorithm used to solve it. Two dual models can be considered (Benali *et al* 1994): a model pertaining to the fundamental curves (called the curve model) and a model pertaining to the fundamental images (called the image model). Both models assume that the fundamental curves and the fundamental images belong to the study space $\mathbb{S}$ resulting from the orthogonal analysis. The curve model assumes that the fundamental curves can be written:

$$\tilde{f}_k(j) = \frac{x_{.j}}{x_{..}} + \sum_{q=1}^{K-1} \frac{1}{x_{..}} \beta_{kq} \varphi_q(j) \tag{A1}$$

where the β_{kq} are the coordinates of the fundamental curve $\tilde{f}_k$ in the study space. Using this model, the fundamental images are given by

$$\tilde{a}_k^*(i) = \gamma_{k0} \frac{x_i^*}{x_{..}} + \sum_{q=1}^{K-1} \frac{1}{x_{..}} \gamma_{kq} \psi_q^*(i) \tag{A2}$$

where the γ_{kq} are the coordinates of the fundamental image $\tilde{a}_k^*$ in the study space. The image model can be deduced from the curve model by substituting variable j for variable i. It assumes that the fundamental images can be written

$$\tilde{a}_k^*(i) = \frac{x_i^*}{x_{..}} + \sum_{q=1}^{K-1} \frac{1}{x_{..}} \gamma_{kq} \psi_q^*(i). \tag{A3}$$

The fundamental curves are then given by:

$$\tilde{f}_k(j) = \beta_{k0} \frac{x_{.j}}{x_{..}} + \sum_{q=1}^{K-1} \frac{1}{x_{..}} \beta_{kq} \varphi_q(j). \tag{A4}$$

Either model is solved in an iterative manner, using non-negativity constraints, normalization constraints and *a priori* knowledge. We give here the relationships holding for the curve model and the image model when correspondence analysis is used for the orthogonal analysis. If another orthogonal decomposition is performed, the gist of the oblique analysis is basically the same but the relationships (especially those related to normalization) are different.

In the curve model, the fundamental image coordinates γ_{kq} are related to the fundamental curve coordinates β_{kq} by

$$\beta\gamma^t = K\,\mathrm{Id} \tag{A5}$$

where β is the $K \times K$ matrix of β_{kq} with the first column $\{\beta_{k0}\}_{k=1,K}$ being set to 1 and γ is the $K \times K$ matrix of γ_{kq} with the first column $\{\gamma_{k0}\}_{k=1,K}$ being set to 1. Id is the $K \times K$ identity matrix.

Moreover, one can show that the following 'normalization' constraints hold:

$$\sum_{k=1}^{K} \beta_{kq}\gamma_{k0} = 0 \qquad \forall q = 1, K-1 \tag{A6}$$

$$\sum_{k=1}^{K} \gamma_{kq} = 0 \qquad \forall q = 1, K-1 \tag{A7}$$

and

$$\sum_{k=1}^{K} \gamma_{k0} = K. \tag{A8}$$

In the image model, the fundamental image coordinates γ_{kq} are also related to the fundamental curve coordinates β_{kq} by equation (A5). The 'normalization' constraints are

$$\sum_{k=1}^{K} \gamma_{kq} \beta_{k0} = 0 \qquad \forall q = 1, K-1 \tag{A9}$$

$$\sum_{k=1}^{K} \beta_{kq} = 0 \qquad \forall q = 1, K-1 \tag{A10}$$

and

$$\sum_{k=1}^{K} \beta_{k0} = K. \tag{A11}$$

When the curve model is used, the algorithm is as shown below:

(1) Initialization of the coordinates β_{kq} of the fundamental curve $\tilde{f}_k$. $\beta_{k0} = 1$ for all curves $\tilde{f}_k$.

(2) Calculation of the corresponding γ_{kq} using equation (A1).

(3) If some of the γ_{kq} are known *a priori*, substitution of the corresponding estimated γ_{kq} values by the known values γ_{kq}.

(4) Normalization of the γ_{kq} so that equations (A3) and (A4) are verified.

(5) Non-negativity constraints on the factor images: the images $\{a_k^*(i)\}_{i=1,N}$ corresponding to the γ_{kq} values are calculated. If $a_k^*(i) < 0$, $a_k^*(i)$ is set to zero. After these substitutions, the new γ_{kq} are deduced and normalized so that equations (A3) and (A4) are verified.

(6) Calculation of the curve coordinates β_{kq} corresponding to the new image coordinates γ_{kq} using equation (A1).

(7) If some of the β_{kq} are known *a priori*, substitution of the corresponding estimated β_{kq} values by the known values β_{kq}.

(8) Non-negativity constraints on the factors: the images $\{f_k(j)\}_{j=1,P}$ corresponding to the γ_{kq} values are calculated. If $f_k(j) < 0$, then $f_k(j)$ is set to zero. After these substitutions, the new β_{kq} are deduced and normalized so that $\beta_{k0} = 1$.

(9) Back to step (2).

The algorithm starts from an initial estimate of the factor coordinates (step (1)). The corresponding factor image coordinates are deduced (step (2)). In some applications, some factor images may be known *a priori*. In this case, the corresponding estimated factor images are replaced by the known factor images (step (3)). After this substitution, the normalization constraints are applied to make sure that the set of factor image coordinates is consistent (step (4)). The next step checks that, given the factors, the associated factor images contain only non-negative values. If they do not, all negative values are replaced by zero. Again, the normalization constraints are applied to ensure that the resulting set of factor image coordinates is consistent (step (5)). Using these new factor images, the corresponding factors are then calculated (step (6)). If some factors are known *a priori*, the corresponding estimated factors are replaced by the known factors (step (7)). All negative factor values are replaced by zero (step (8)). After these substitutions, the factors are normalized so that the set of factor coordinates is consistent with the normalization constraints. The resulting

factors can then be used to get new estimates of the fundamental images. The procedure is repeated until a stopping criterion is met. The stopping criterion can be: (i) a default number of iterations; (ii) a number of negative values in the factor images or in the factors less than a given threshold; (iii) a change between two consecutive factor images or factor coordinate estimates less than a given threshold.

When solving the image model instead of the curve model (Benali *et al* 1994), the iterative procedure is the same except that it starts from an estimate of the factor images. Furthermore, the normalization constraints are those related to the image model, i.e. corresponding to equations (A10) and (A11), instead of being those given by equations (A7) and (A8).

References

Barber D C 1980 The use of principal components in the quantitative analysis of gamma camera dynamic studies *Phys. Med. Biol.* **25** 283–92

Benali H, Buvat I, Frouin F, Bazin J P and Di Paola R 1993 A statistical model for the determination of the optimal metric in factor analysis of medical image sequences (FAMIS) *Phys. Med. Biol.* **38** 1065–80

——1994 Foundations of factor analysis of medical image sequences *Image Vision Comput.* **12** 375–85

Buvat I, Rodriguez-Villafuerte M, Todd-Pokropek A, Benali H and Di Paola R 1995 Comparative assessment of nine scatter correction methods based on spectral analysis using Monte Carlo simulations *J. Nucl. Med.* **36** 1476–88

Caussinus H 1986 Models and uses of principal component analysis *Multidimensional Data Analysis* ed J de Leeuv (Leiden: DSWO Press) pp 149–78

Di Paola R, Bazin J P, Aubry F, Aurengo A, Cavailloles F, Herry J Y and Kahn E 1982 Handling of dynamic sequences in nuclear medicine *IEEE Trans. Nucl. Sci.* **29** 1310–21

Frouin F, Bazin J P, Di Paola M, Jolivet O and Di Paola R 1992 FAMIS: a software package for functional feature extraction from biomedical multidimensional images *Comput. Med. Im. Graph.* **16** 81–91

Houston A S and Sampson W F D 1997 A quantitative comparison of some FADS methods in renal dynamic studies using simulated and phantom data *Phys. Med. Biol.* **42** 199–217

Kendall M G and Stuart A 1979 *The Advanced Theory of Statistics* (London: Griffin)

Samal M, Karny M, Surova H, Marikova E and Dienstbier Z 1987 Rotation to simple structure in factor analysis of dynamic radionuclide studies *Phys. Med. Biol.* **32** 371–82

Samal M, Karny M and Zahalka D 1991 Confirmatory aspects in factor analysis of image sequences *Information Processing in Medical Imaging* ed A C F Colchester and D J Hawkes (Berlin: Springer) pp 397–407

——1993 Bayesian identification of a physiological model in dynamic scintigraphic data *Information Processing in Medical Imaging* ed H H Barett and A F Gmitro (New York: Springer) pp 422–37

Samal M, Surova H, Karny M, Marikova E, Penicka P and Dienstbier Z 1988 The reality and meaning of physiological factors *Information Processing in Medical Imaging* ed C De Graaf and M Viergever (New York: Plenum) pp 499–519

Wu H M, Hoh C K, Buxton D B, Kuhle W G, Schelbert H R, Choi Y, Hawkins R A, Phelps M E and Huang S C 1995 Quantification of myocardial blood flow using dynamic nitrogen-13-ammonia PET studies and factor analysis of dynamic structures *J. Nucl. Med.* **36** 2087–93